

A-type carbonate in strontium phosphate apatites

Revision 2

Melissa M. Bollmeyer, Molly C. Carney, Claude H. Yoder*

Department of Chemistry, Franklin and Marshall College, Lancaster, Pennsylvania 17603,

United States

*corresponding author cyoder@fandm.edu 717-358-3806

Abstract

One of the most important characteristics of the apatite family of minerals is its ability to undergo substitution by ions such as sulfate and carbonate. The substitution of carbonate is particularly important because of the presence of carbonate in bone mineral and the recent suggestion that most of the substituted carbonate resides in the apatite channels (A-type substitution) rather than in place of phosphate (B-type substitution). The possibility of additional channel species or environments in carbonated Ca hydroxylapatite has been pursued via its Sr homolog, which is known to have a larger channel volume and a greater unit cell a-axial length than its unsubstituted parent. Strontium hydroxyl-, chlor-, and fluorapatites, containing incorporated ^{13}C -carbonate up to 7 wt%, were synthesized by aqueous precipitation reactions in the presence of Na, K, and ammonium counter cations. ^{13}C -labeled carbonate was used to facilitate observation of the solid-state ^{13}C MAS NMR spectra. Band-fitting of the IR carbonate asymmetric stretch ν_3 region required the use of eight bands, arranged as four doublets, that are interpreted as representing three channel environments (A-type substitution) and one B-

type substitution. The carbonate ν_3 region of low Na, carbonated Sr hydroxylapatite contained the high frequency limbs of the A-type doublets in the area between 1520 cm^{-1} and the B-type region ($1400\text{-}1360\text{ cm}^{-1}$), whereas in the high Na analog the A-type doublets produced a broad high frequency tail into the B-type region. Similar behavior was exhibited by the chlor- and fluorapatite analogs. Heating samples to $600\text{ }^\circ\text{C}$ resulted in loss of carbonate and conversion to A-type carbonate demonstrating the stability of A-type carbonate at higher temperatures.

Analysis of the populations of A-, A'-, and A''-, and B-sites for the hydroxyl-, chlor-, and fluorapatites, prepared under both low Na and high Na conditions, revealed that high Na/carbonate ratios produce a larger amount of channel substitution, contrary to observations for Ca homologs. It is speculated that multiple A-environments also exist for Ca hydroxylapatite prepared by aqueous precipitation, which is consistent with Fleet's analysis of apatite prepared at high temperature and pressure.

Introduction

The apatite family of minerals has the distinction of having members (Ca hydroxylapatite) of biological necessity to vertebrates and ions, such as Ca, Sr, phosphate, and hydroxide, that can be easily substituted. These characteristics can be partly rationalized by the abundance of the constituent ions and the hexagonal structure containing close-packed phosphate ions and cations that form channels that can accommodate anions and neutral molecules (Hughes and Rakovan 2002). The possibility of ion mobility in the channel that gives rise to nutrition and acid-base regulation (Fleet 2017) makes it particularly intriguing. The carbonate ion is known to substitute for two

hydroxide ions located in the channel (A-type substitution) and also for phosphate (B-type substitution) (Pan and Fleet 2002). At least two types of channel carbonate ions with different orientations have been identified by X-ray diffraction (Fleet 2015; Fleet 2017) and three different environments for channel carbonate have been postulated on the basis of IR spectra (Fleet 2017).

Carbonated Ca hydroxylapatite, a close approximation to the inorganic material that constitutes bones and teeth, has been thought to contain primarily B-type carbonate, with A-type contributing not more than 10-15% of the total carbonate (Elliott 2002). Those assumptions were challenged by Fleet (2017) in an analysis of the IR spectra of Na-containing apatite prepared at high temperature and pressure. This disentanglement of the carbonate asymmetric stretch region (ν_3) of the IR spectrum, a frequently used monitor of the types of carbonate in apatite, suggested that the use of spectral indicators of A-type carbonate must be replaced by careful band-fitting, especially in this complex region of the IR.

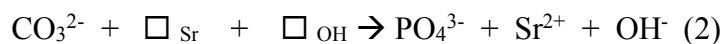
All of the alkaline earth metal cations except those of Be and Mg form apatites that are structurally homologous to those of Ca but with more voluminous channels. Strontium, the closest homolog to Ca, forms apatites that have been used to enhance bone remediation and are closely related in structure and properties to their biologically active Ca counterparts. It is natural to speculate therefore on the possibility of additional carbonate ion orientations in the Sr apatite channel, or to propose different channel environments.

We have previously shown that the a-axial length for carbonated Sr hydroxylapatite increases with increasing carbonate substitution and that the carbonate

asymmetric stretch region of the IR spectra for these compounds exhibits two sets of doublets (Weidner et al. 2015). Both observations, and those of Jebri et al. (2012, 2013), suggest that the Sr homolog of carbonated Ca hydroxylapatite contains considerably more A-type carbonate. In this study, we examine the IR and solid-state NMR spectra of a series of carbonated Sr hydroxyl-, chlor-, and fluorapatites that have been prepared by aqueous precipitation reactions using ammonium, Na, or K counter ions. The counter cation ($M^+ = \text{NH}_4^+, \text{Na}^+, \text{K}^+$) in these reagents may undergo co-substitution with carbonate:



but charge-balance may also occur with the formation of vacancies (\square),



or, with accompanying hydroxide.



We have also made use of ^{13}C -labeled carbonate to facilitate the observation of ^{13}C solid state NMR spectra. We anticipate that our results will be of particular value in setting a broader context for A-site carbonate comparisons with Ca hydroxylapatite and in understanding channel substitution in other apatites as well.

Experimental Section

For all syntheses, Milli-Q deionized water and ACS reagent grade reagents with purities of above 98% were used. ^{13}C -labelled CO_2 with 99% purity was obtained from Sigma-Aldrich. Labeled ^{13}C - NaHCO_3 was obtained from Sigma-Aldrich. Percent yields for the aqueous preparation of carbonated Sr apatites were > 90%. Each apatite was

obtained in at least two independent syntheses and was characterized by multiple IR and NMR analyses.

Carbonated Sr hydroxylapatite (CSrApOH)

Two carbonated Sr hydroxylapatites were prepared in the presence of varying Na-containing reagents (low and high) during synthesis. A 25 mL solution of 0.22 M $\text{Sr}(\text{NO}_3)_2$ and a 25 mL solution of 0.13 M $\text{NH}_4\text{H}_2\text{PO}_4$ (low-Na) or $\text{Na}_3\text{PO}_4 \cdot 12\text{H}_2\text{O}$ (high-Na), were added simultaneously at a rate of 1 drop/sec to a 25 mL solution of 0.091 M ^{13}C -labelled NaHCO_3 . The reactions were heated to 90°C and the pH was maintained at 9 using 3 M NH_3 (low-Na) or 3 M NaOH (high-Na). After the digestion time of two days, the products were filtered, washed 4 times with 30 mL of distilled water, and dried in a vacuum oven at 5 torr and room temperature for 12 hours. A non-carbonated sample was prepared by adding the Sr solution drop-wise to the phosphate solution under the same conditions. In the text and tables the identity of samples is given in parentheses.

Low, medium, and high Na-containing samples were also prepared using the same procedure with unlabeled Na bicarbonate. The same procedure was followed for K-containing, Sr hydroxylapatite samples, where $\text{NH}_4\text{H}_2\text{PO}_4$ and K_2CO_3 were used for the low-K sample, and K_2HPO_4 and K_2CO_3 were used for the high-K sample. These mixtures were digested for four days, and the pH was kept at 9 using 3 M NH_3 . A sample was also prepared using only ammonium salts ($\text{NH}_4\text{H}_2\text{PO}_4$ and $(\text{NH}_4)_2\text{CO}_3$).

Carbonated Sr fluorapatite (CSrApF)

Two carbonated Sr fluorapatite samples were prepared in the presence of different amounts of Na (low and high). A 25 mL solution of 0.22 M $\text{Sr}(\text{NO}_3)_2$ and a 25 mL solution of 0.13 M $\text{NH}_4\text{H}_2\text{PO}_4$ (low-Na) or $\text{Na}_3\text{PO}_4 \cdot 12\text{H}_2\text{O}$ (high-Na), were added simultaneously at a rate of 1 drop/sec to a 25 mL solution of 0.091 M ^{13}C -labelled NaHCO_3 and 0.13 M NH_4F (low-Na) or NaF (high-Na). The reactions were heated to 80 °C and the pH was maintained at 8 using 3 M NH_3 . After the digestion time of one day, the products were filtered, washed 4 times with 30 mL of distilled water, and dried in a vacuum oven at 5 torr and room temperature for 12 hours.

Carbonated Sr chlorapatite (CSrApCl)

Two carbonated Sr chlorapatite samples were prepared in the presence of different amounts of Na (low and high). A 50 mL solution of 0.23 M SrCl_2 and a 50 mL solution of 0.14 M $\text{NH}_4\text{H}_2\text{PO}_4$ (low-Na) or $\text{Na}_3\text{PO}_4 \cdot 12\text{H}_2\text{O}$ (high-Na), were added simultaneously at a rate of 1 drop/sec to a 25 mL solution of 0.14 M ^{13}C -labelled NaHCO_3 . The reactions were heated to 80°C and the pH was kept at 9 using 3 M NH_3 . After the digestion time of two days, the products were filtered, washed 4 times with 30 mL of distilled water, and dried in a vacuum oven at 5 torr and room temperature for 12 hours.

A-type carbonated Sr hydroxylapatites (A-CSrApOH)

Starting materials, including a non-carbonated apatite and low, medium, and high Na-containing apatites, were finely ground and placed as a thin layer in a ceramic boat. The samples were calcined at 800°C for 7-24 hours and then placed in a quartz tube in a

tube furnace. Activated (350°C) molecular sieves were placed in flasks at both ends of the tube, and a flow meter and bubbler were connected to the flask at the exit. The tube furnace was heated to 800 °C, and CO₂ was passed over the samples at about 0.1 L/min for 1 day. For ¹³C-labelled CO₂ reactions, the flow rate was 0.2 L/min for 2 hours at 800°C.

Characterization

Powder X-ray diffraction patterns were obtained on a PANalytical X'Pert PRO Multi-Purpose Diffractometer Thea-Theta System with Cu-K α radiation ($\lambda=1.54060$ Å). Samples were prepared on a 32 mm glass slide and were scanned for 45 minutes with a range from 5 to 70° 2 θ . Unit-cell parameters were determined using the PANalytical program X'Pert Highscore Plus from 2.5 h scans using an 8 mm cavity slide.

A Bruker Tensor 37 IR Spectrometer with a Ge ATR mount was used to obtain the IR spectra of products using 256 scans at a resolution of 2 cm⁻¹. For all samples peak-fitting was done on spectra not modified by smoothing or base-line correction using Thermo Scientific GRAMS/AI Spectroscopy Software Suite. Peak fitting of the asymmetric carbonate stretch region (ν_3) was based on the model that the spectral envelope is a sum of intensity due to two to four underlying doublets, the members of which are nearly equally intense. This method is based on the assumption that both A- and B-type carbonate ions have less than D_{3h} symmetry in the apatite structure. Each structurally different ion therefore gives rise to two asymmetric stretch and one out-of-plane bend bands. The use of Gaussian functions for both the carbonate asymmetric stretch region (ν_3) and the out of plane bend region (ν_2) accounted for at least 96% of the spectral

intensity for most samples. The average standard error for the peak-fitting was 0.0011. Populations of A-, A'-, A''-, and B- carbonate environments were obtained from band areas assuming that the extinction coefficients for each band were the same. The uncertainties in populations of these environments were determined from at least 3 separate series of peak-fittings and are, on average, 9% of the population. The uncertainties in percentages (the square root of the sum of the variances for each peak type) for apatite (12) are A (6), A' (18), A'' (18), and B (10), and for apatite (15) are A (11), A' (8), A'' (10), and B (8). In the spectral figures, dotted lines represent the experimental spectra and solid lines represent Gaussian or Lorentzian curves or the best-fit sums of those functions.

Solid-state NMR spectra were obtained using an Agilent Unity 500 MHz NMR spectrometer equipped with a 3.2 mm solids probe capable of spin speeds of 24 kHz. ^{13}C and ^{19}F spectra were obtained at 125.15 MHz and 469.673 MHz respectively, using delay times of 100 and 10 sec, respectively. ^{13}C spectra were referenced to adamantane at 37.4 ppm, and ^{19}F spectra were referenced to NaF at -122.0 ppm.

Weight percent Na for some samples was obtained using X-ray fluorescence spectroscopy (XRF) with a Panalytical PW 2404 Vacuum Spectrometer equipped with a 4kW Rh X-ray tube. An anhydrous powder of each sample was prepared by ignition at 1200 °C, and then used to prepare a glass disc with one part anhydrous sample material and 9 parts Li tetraborate. Percent Na for some samples, as well as percent carbonate for all samples were determined by combustion analysis using a Costech ECS4010 CHNSO Analyzer and by Galbraith laboratories (Knoxville, TN).

Results

All products were examined by XRD and contained no SrCO₃ at percentages above ca. 0.3 wt%. The use of mole ratios of 0.8 mole carbonate (and larger) to 1.0 mole phosphate in the synthesis of the Sr apatites was found to produce SrCO₃.

A-type carbonated apatites

The synthesis of A-type carbonated, Sr hydroxyl-, chlor-, and fluorapatites has been discussed by Walleyes (1954), Bonel (1972), and Yoder et al. (in review 2018). The ¹³C isotopomers of these apatites have been characterized by IR, NMR, and unit cell parameter analyses (Yoder, in review 2018). For reference, the carbonate IR peak positions and NMR chemical shifts are recorded in Table 1.

Carbonated Sr hydroxylapatite (CSrApOH)

The asymmetric carbonate stretch (ν_3) region of the IR spectrum of low Na¹³C-SrApOH (12), containing 4.4 wt % carbonate and 0.8 wt %Na, prepared by aqueous precipitation using only NaH¹³CO₃ as a Na-containing starting material, contains peaks for both A- and B-type carbonate (Fig. 1). The peak at 1507 cm⁻¹ and the most intense peaks in the spectrum at 1396 and 1365 cm⁻¹ are assigned to the high frequency limb of an A-type doublet (1507 cm⁻¹) and a B-type carbonate doublet, respectively. The corresponding peak positions for an apatite containing natural abundance carbonate would appear at approximately 1545, 1434, and 1403 cm⁻¹, which can be compared with the A- and B-type frequencies given for synthetic Ca analogs at 1462 ± 5 and 1535 ± 6 cm⁻¹ for A-type carbonate, and 1420 ± 6 and 1458 ± 5 cm⁻¹ for B-type carbonate (Tacker

2008).

In the region between 1507 and 1396 cm^{-1} there is considerable spectral amplitude with small peaks at 1470 and 1437 cm^{-1} . We assign bands at these positions to A' and A'' carbonates. The assignment of peaks at 1507, 1470, and 1437 cm^{-1} to the high frequency limbs of three A-type doublets is based on: a) the peak frequencies, which are distinctly higher than those for the B-region; b) the observation of differences ($\Delta\nu$) between high and low frequency bands in the range of 70-107 cm^{-1} for A-type peaks, compared to a range of 25-55 cm^{-1} for B-type peaks in carbonated, Ca hydroxylapatites (Fleet 2015; Yoder et al. in review 2018); and c) the necessity to use bands of appropriate width (ca. 20-40 cm^{-1}) to account for all of the spectral intensity in the spectral envelope (see also the Discussion section). Hereafter, the multiple A-bands will be referred to as sites. Thus, the A-type carbonate ions may exist in A-, A'-, and A''-sites.

Band-fitting was therefore based on a four species model derived from the appearance of the ν_3 carbonate region and the solid-state ^{13}C NMR spectrum (see below). Assuming that all carbonate ions in apatite have less than D_{3h} symmetry, each stereochemically-distinct carbonate ion should exhibit a doublet in the ν_3 region and a singlet in the ν_2 region. For three different A-type carbonates, the ν_3 region should contain a total of 8 bands, two for each A-type carbonate and two for the one B-type carbonate ion, while the ν_2 region should contain four bands, one for each species.

The positions of the bands in the ν_2 region do not vary in the same way as those in the ν_3 region. There are two A-type carbonate ions with bending motions at higher frequencies than the B-type, but one (A'') is at lower frequency (cf. Fleet 2015). Table 2

contains the positions of all bands in this model as well as their areas as percentages of the whole region. It also contains band positions and populations for all of the apatites in this study. The agreement in populations of the ν_3 and ν_2 areas is within several percent.

In order to compare the ν_2 band positions to literature values for A- and B-type carbonate in Ca apatites the values in Table 2 can be adjusted by adding 26 cm^{-1} (the difference between the ν_2 values in Table 1 for natural abundance vs ^{13}C -labeled CSrApOH). The converted values are 877 and 870 cm^{-1} for the bands assigned to A- and B-type carbonate, respectively, in good agreement with the generally accepted ν_2 region ranges of $880\text{-}878 \text{ cm}^{-1}$ for A-type and $873\text{-}871 \text{ cm}^{-1}$ for B-type (Fleet 2017). The total A-type carbonate in (12) can be estimated at slightly greater than 50%, in sharp contrast to the 5 – 9% reported for Na-bearing Ca hydroxylapatite (Yoder et al. in review 2018).

The NMR ^{13}C spectrum (Fig. 2) contained three peaks as well as a shoulder on the high frequency side. This spectrum was verified for three independent preparations of the apatite. The spectrum was fitted with four peaks, with the lowest frequency peak (165.2 ppm) being assigned to A-type carbonate based on the chemical shift of 164.1 ppm for pure A-type (Table 1). The assignments (Table 2) of the other peaks were based on the IR carbonate ν_3 band populations.

The IR spectrum of the high Na apatite ^{13}C -SrApOH (15), containing 7.0 wt % carbonate and 1.0 wt % Na, has a ν_3 region that shows small A-type bands (Fig. 3) at 1508 and 1415 cm^{-1} with highly populated A'' bands at 1428 and 1351 cm^{-1} .

Although this general appearance of the ν_3 region is sometimes assumed to be indicative of B-type carbonate substitution in Ca apatites (Roux and Bonel 1980; Vignoles, et al. 1988), the band positions and populations given in Table 2 for ^{13}C -

SrApOH (15) indicate that B-type carbonate is only 36% of the total amount of carbonate. This can be compared to the 48% B-type carbonate in low Na-bearing CSrApOH (12). Hence, an increase in carbonate content in Sr hydroxylapatite leads to a decrease in the percentage of B-type carbonate.

The solid state MAS NMR spectrum of ^{13}C -CSrApOH (15) (Fig. 4) contains a single peak with a significant tail on the low chemical shift side. This spectral envelope accommodates the four bands used in the fitting of the IR ν_2 region, with the band for the A-site carbonate at the chemical shift (166.2 ppm) close to the chemical shift of 164.1 ppm for the pure A-type (Table 1). The chemical shift assigned to type-B carbonate (168.5 ppm) is similar to that given above (167.9 ppm) for ^{13}C -CSrApOH (12).

Carbonated Sr fluorapatite (CSrApF)

The asymmetric stretch carbonate (ν_3) and out-of-plane bend (ν_2) regions of the IR spectrum of apatite ^{13}C -CSrApF (71), which contains 3.2 wt % carbonate and 0.6 wt % Na, are shown in Figure 5. This sample was prepared by the reaction of $\text{Sr}(\text{NO}_3)_2$ and $\text{Na}_3\text{PO}_4 \cdot 12\text{H}_2\text{O}$ with a mixture of ^{13}C -labeled NaHCO_3 and NaF . Because three reagents contained the Na counter ion, the product ^{13}C -CSrApF (71) was expected to contain more Na than the product of the same reaction using $\text{NH}_4\text{H}_2\text{PO}_4$ and NH_4F . In fact, the low Na ^{13}C -CSrApOH (65) does contain less Na and carbonate, but the IR spectra of ^{13}C -CSrApF (71) and ^{13}C -CSrApOH (65) are nearly identical.

Because the ν_3 region does not contain a band for A-type carbonate, six bands were used to account for all of the species in the ν_3 region and three bands were utilized for ν_2 (Fig. 5, Table 2). Based on the frequency of A-site bands in apatites ^{13}C -

CSrApOH (12) and ^{13}C -CSrApOH (15) the highest frequency band was assigned to an A'-site, which led to an assignment of the second highest frequency band as A''.

Fortunately, the lowest frequency peak in the ν_2 region (837 cm^{-1}) can be confidently assigned to B-type carbonate, even though the frequency is 8 cm^{-1} below that of B-type in ^{13}C -CSrApOH (12) and ^{13}C -CSrApOH (15).

The solid state NMR spectrum of ^{13}C -CSrApF (71) (Fig. 6) contains a single peak with significant intensity asymmetry to the low frequency side. This intensity envelope can be fit with three peaks, whose occupancies (Table 2) are in good agreement with those obtained from the ν_3 and ν_2 carbonate regions of the IR spectrum.

Carbonated Sr chlorapatite (CSrApCl)

The carbonated low Na-bearing chlorapatite, ^{13}C -CSrApCl (57) was obtained in the reaction of SrCl_2 with $\text{NH}_4\text{H}_2\text{PO}_4$, and ^{13}C -labelled NaHCO_3 and contains 3.75 % CO_3 , 0.4 % Na, and 0.05 % Cl. The carbonate ν_3 and ν_2 regions of the IR spectrum (not shown) are similar to those of low Na ^{13}C -SrApOH (12) (Fig. 1). Table 2 contains band frequencies and populations for both regions. The solid state MAS ^{13}C NMR spectrum is shown in Figure 7, while the corresponding chemical shifts and populations are given in Table 2.

A calculation of the amount of channel carbonate using the total wt % carbonate of 3.75 and the approximately 60% A-type carbonate based on the ν_2 populations shows that there is roughly 60% of the 1 mole predicted by the idealized formula of $\text{Sr}_{10}(\text{PO}_4)_6\text{CO}_3$. The channel also contains a very small amount of chloride, but the

remainder is likely hydroxide, a result of the aqueous preparation and the formation of a hydroxide, chloride solid solution.

The IR (not shown) and NMR spectra (Fig. 8) of the high Na-bearing ^{13}C -CSrApCl (58) are quite different than those of the low Na-bearing ^{13}C -CSrApCl (57), but similar to those of the high Na ^{13}C -CSrApOH (15) (Fig. 3).

Discussion

The carbonate ν_3 and ν_2 regions of the IR spectra and the ^{13}C NMR patterns of our Sr carbonated apatites contain features that are not easily explained on the basis of the presence of two substituting species, the A- and B-type carbonate ions. Attempts at band-fitting, assuming only two or three species, resulted in major portions of the IR and NMR carbonate spectral envelopes that were not accounted for. The use of less than four carbonate species for band-fitting of the IR ν_3 region also produced: a) bands that are significantly wider than the widths of pure A-type bands, which have widths (FWHM) of approximately 25 cm^{-1} ; b) distances ($\Delta\nu$) between members of the high frequency doublet that are significantly lower than the $\Delta\nu = 91\text{ cm}^{-1}$ observed for peaks in pure A-type CSrApOH (12); c) band positions that are more than 10 cm^{-1} lower than the positions of the peaks for A-type carbonate bands in CSrApOH (12); and d) doublets that have widely disparate areas (area ratios that differ by more than about 25%) for their two limbs. Band-fitting based on a four species model accounts for all features, except, in some cases, for slight (generally less than 5% of the total spectral envelope) pre- and post-peak tailing in the IR spectra.

The positions of the small peaks in the carbonate ν_3 region of the IR spectrum at frequencies higher than those of the accepted B-type region of approximately 1410 -1460 cm^{-1} (for ^{13}C , approximately 1370-1420 cm^{-1}) we assign with some confidence to A-type carbonate. All of the low Na-bearing Sr apatites prepared in this study exhibit definite peaks between the B-region and 1507 cm^{-1} (observed for the high frequency member of the doublet for pure A-type ^{13}C -SrApOH). Of the four low Na apatites prepared (most synthesized two or three times using the same synthesis procedure and conditions), all showed three peaks (see Fig. 1, add 38 cm^{-1} to the peak positions to obtain wavenumbers for the unlabeled analog) between the B-region and 1507 cm^{-1} . We assume therefore that most low and high Na-bearing Sr apatites contain A-type carbonate ions in three different environments. These carbonate ions could be non-equivalent as a result of different structural features or different orientations in the channel, but in the absence of X-ray diffraction data, we assume that the ions likely have the same structure and similar orientations in the channel. Because vibrational and NMR spectra are sensitive to the environment of the group or nucleus being observed, we believe that the differences between these channel ions seen in IR and NMR spectra can be attributed to different environments. This is consistent with the model of Fleet (2015, 2017) for Na-containing Ca homologs. The different environments are a result of the charge-balance mechanisms that control the aqueous precipitation of B-type carbonate substituted apatite, and may include a vacancy (Reaction 2) or a counter ion (Reaction 1) originally present with an anion in a synthesis reagent. Assuming that the changes expressed by equations 1 and 2 occur in the channel, Table 3 shows some possibilities for the structure of the channel walls following B-type carbonate substitution.

When A-type substitution occurs in the absence of B-type substitution, each carbonate replaces two hydroxide ions present in the channel of the parent apatite and therefore a given channel carbonate ion is surrounded by the six Sr^{2+} ions that make up the channel wall (see Fig. 9). We attribute the asymmetric stretch doublet with the highest frequency in the ν_3 region of the IR spectrum of our apatites to a carbonate ion in this channel environment (the A-site). The second highest frequency doublet is assigned to the asymmetric stretching of a carbonate ion of the same structure in a channel in which it is surrounded by five Sr^{2+} ions and one Na^+ ion (the A'-site). A carbonate ion with the third highest frequency doublet is assumed to be present in channels that contain either four Sr^{2+} ions and two Na^+ ions or five Sr^{2+} ions and one vacancy (the A''-site). As noted in Table 3, both environments provide the same overall charge. These assignments are based on the overall charge in the surrounding channel, and are consistent with our previous density functional theory calculations, which indicate that the frequency of the asymmetric stretch of carbonate decreases as the charge density of the cation decreases (Yoder, et al. in review 2018). The assignments are shown in Table 2 for apatites CSrApOH (12) and CSrApOH (15).

It is clear that the frequencies of the bands for the pair CSrApOH (12) and CSrApOH (15) are very similar, but differ in the populations of their environments. For example, the population of the A-environment decreases from 15% in low Na CSrApOH (12) to 5% in high Na CSrApOH (15), while the population of the A''-environment increases from 22 to 39 %. These changes make the ν_3 region of the high Na apatite appear as a horizontally compressed version of the ν_3 region of the low Na apatite. The same “compression” can be seen in the NMR spectra of CSrApOH (12) and CSrApOH

(15) and in a comparison with the ν_3 region from the IR spectra of Na-free relative to Na-bearing Ca apatites synthesized at high temperature and pressure (Fleet, 2017, Fig. 3). The decrease in the population of the A-site and increase in the A''-site can be attributed to the greater amount of carbonate and Na ions in CSrApOH (15). For a carbonate ion occupying these sites (A' and A'') the charge experienced is lower than that of a carbonate in the A-site. The observation of increased B-type substitution in Ca apatites (Vignoles, et al. 1988, Barralet, et al., 1998), as the total percentage of carbonate increases, could be attributed to this decrease in the A-site charge (but see below).

The data in Table 2 show that in high Na CSrApOH (15), the percentage of B-type substitution is lower than that in low Na CSrApOH (12). In fact, the percentage of B-type carbonate in the more highly carbonated apatite is also lower than that in the less carbonated apatite for every hydroxyl-, chlor-, and fluorapatite that we have studied (Table 4). Our results indicate that although the decrease in channel charge due to greater carbonation may decrease the stability of A-type substitution, A-type substitution is still favored at high carbonate/Na ratios in Sr apatites. Whether our generalization is true only for Sr apatites or is more generally applicable to both Ca and Sr apatites is not certain. The observation, that increased carbonate leads to greater B-type carbonate in Ca apatites, is applicable to the Sr apatites in the present study if "greater B-type substitution" refers to amount of carbonate and not percentage carbonate. This observation appears, however, to have been based mainly on the use of "signature" peaks (e.g., 1545 cm^{-1} as A-type carbonate) rather than from the use of deconvolution to determine the substitution type. Given the compression that occurs in the appearance of the ν_3 region of the IR

spectrum of highly carbonated Sr apatites, it is reasonable to assume that these, as well as highly carbonated Ca apatites, could be mistaken as primarily B-type regions.

In order to determine if the compression of the ν_3 region at high carbonate concentrations is due primarily to Na ions or to the accompanying carbonate ions, we have also used ammonium and K salts in the preparation of several apatites. The ν_3 regions of the IR spectra of these apatites, all of which contain between 6.5 and 7.2% carbonate, along with the high carbonate/high Na ratio CSrApOH (15) are shown in Figure 10. It is clear that the ν_3 regions of the apatites, except CSrApOH (15), are very similar (CSrApOH (72) shows a bit more A-type carbonate than the others. The ν_3 region of high carbonate CSrApOH (72) (7.2 % carbonate, 0.05 % K), which contains a very small amount of K, and the high carbonate CSrApOH (64) (6.5 % carbonate, %N < 0.5%), which contains a small amount of ammonium ion, have the same appearance as the low carbonate, low Na CSrApOH (12). Because the ν_3 regions are similar for all but CSrApOH (15), which contains a greater amount of Na, it is likely that the presence of Na ion, rather than just carbonate, is responsible for the compressed appearance (lower frequency A and the greater population of A'' environments) of the high carbonate apatites. Because it is not possible using our synthetic conditions to incorporate a large amount of NH_4^+ and K^+ ions, the role of other counter ions cannot be explored.

The relative stabilities of the three A-sites (A, A', A'') is reflected in their behavior on heating to 600 °C for 12 hours. The carbonate ν_3 region of the IR spectrum of low Na CSrApOH (44) is shown before and after heating in the top portion of Figure 11. Because the spectra are normalized to the phosphate peak, it is clear that the ν_3 region has less area after heating, indicating partial decomposition of carbonate to CO_2 .

More importantly, the A- and B-content of the apatite has been reorganized by an increase in A-site carbonate at the expense of A', A'', and B-site carbonate. The bottom portion of Figure 11 contains the ^{13}C NMR spectrum of low Na CSrApOH (44) before and after heating. There was no indication of A-site carbonate in the ^{13}C NMR spectrum of high Na CSrApF (71), whereas in the heated sample the A-site peak was definitely present. This is apparently a manifestation of the greater stability of the more highly charged six Sr cation environment for the A-type carbonate.

Implications

The ionic radius of Sr^{2+} (1.18 Å) is about 20% larger than that of Ca^{2+} (1.00 Å) and the Sr chlor- and hydroxylapatites contain about 10% greater number of water molecules per unit cell (Goldenberg, et al., 2015), suggesting that the channels in Sr apatites might accommodate more carbonate ions than their Ca analogs. Indeed, the model of three A-sites for Na-containing carbonated Sr hydroxylapatite is necessary for the rationalization of the IR and NMR spectra of Sr apatites and represents the first detailed examination of the IR and NMR spectra of Sr apatites. Though the difference in these sites could be attributed to structural differences within the carbonate ions or to geometric differences in orientation in the channel, we attribute the difference to the location of carbonate in different channel environments (Fleet 2017). We have applied this “channel environments” model to the IR spectra of carbonated Sr and Ca apatites, and have successfully used the same model to account for the multiple peaks in the carbonate region of the ^{13}C NMR solid-state spectra of these same compounds.

Although these environments are more clearly observed in the IR and NMR spectra of Sr apatites, due to the greater dispersion of IR frequencies and NMR chemical shifts in their spectra, we are persuaded that even Ca apatites contain A-type carbonate ions in more than one different environment. These environments were first postulated by Fleet (2017) in Ca apatites prepared in high temperature/pressure reactions containing Na. The evidence accumulated in our present study, as well as in a recent study (Yoder et al., in review 2018), suggests that Ca apatites synthesized without the use of pressure at temperatures below 100 °C and in the presence of other counter ions may contain a larger percentage of A-type carbonate than previously thought. Deconvolution of the IR spectra of Ca apatites obtained by aqueous precipitation containing only small amounts of Na, using the same models used here, produces much larger A-type populations. For example, the same peak-fitting criteria used for carbonated Sr apatites can account for about 50 % A-type carbonate (as determined from peak areas in the carbonate ν_2 and ν_3 regions) in a Ca apatite (82) (4.1 wt.% carbonate, 0.1 wt.% Na) made by aqueous precipitation (Fig. 12). If carbonate incorporation is the same in apatites precipitated in aqueous solution as those prepared using high temperature and pressure, as suggested by the apatites in the present study, it seems likely that there is even a significant amount of channel carbonate in bone apatite.

Acknowledgements

The authors are indebted to the reviewers, Kyle T. Ashley and XXX, to Stanley and Karen Mertzman and Emily Wilson (Department of Earth and Environment, Franklin and Marshall College) for analytical work, to Kathleen Stepien (Franklin and Marshall College) for technical assistance, to the Camille and Henry Dreyfus Foundation for a

Senior Scientist Mentor award (CHY), and to the Lucille and William Hackman Summer Research Program and the Yoder Student Research Endowment at Franklin & Marshall College for funding.

References

- Bonel, G. (1972) Contribution to the study of the carbonation of apatite. *Annales des Chimie*, 7, 65-87.
- Elliott, J.C. (1994) Structure and chemistry of the apatites and other calcium orthophosphates. 389 p. Elsevier, Amsterdam.
- Fleet, M.E. and Liu, X. (2007) Coupled substitution of type A and B carbonate in Na-bearing apatite. *Biomaterials*, 28, 916-926.
- Fleet, M. (2015) Carbonated hydroxyapatite: Materials, synthesis, and application. 268 p. CRC Press, FI (Taylor and Francis Group).
- Fleet, M. (2017) Infrared spectra of carbonate apatites: Evidence for a connection between bone mineral and body fluids. *American Mineralogist*, 102, 149-157.
- Goldenberg, J.E., Wilt, Z., Schermerhorn, D.V., Pasteris, J.D., Yoder, C.H. (2015) Structural effect on incorporated water in carbonated apatites. *American Mineralogist*, 100, 274-280.
- Hughes, J.M., Rakovan, H (2002) The crystal structure of apatite, $\text{Ca}_5(\text{PO}_4)_3(\text{F},\text{OH},\text{Cl})$, in M. Kohn, J. Rakovan, J., J.M. Hughes, Eds., *Reviews in Mineralogy and Geochemistry*, 48, 1-12.

- Jebri, S., Boughzala, H., Bechrifa, A., Jemal, M. (2012) Structural analysis and thermochemistry of “A” type phosphostrontium carbonate hydroxyapatites. *Journal of Thermal Analysis and Calorimetry*, 107, 963-972.
- Jebri, S., Boughzala, H., Bechrifa, A., Jemal, M. (2013) Rietveld structural refinement of “A” type phosphostrontium carbonate hydroxyapatites. *Powder Diffraction*, 28, S409-S424.
- Madupalli, H., Pavan, B., Tecklenburg, M. (2017) Carbonate substitution in the mineral component of bone: discriminating the structural changes, simultaneously imposed by carbonate in A and B sites of apatite. *Journal of Solid State Chemistry*, 255, 27-33.
- Pan, Y., Fleet, M.E., (2002) Compositions of the apatite-group minerals: substitution mechanisms and controlling factors, in M. Kohn, J. Rakovan, J., J.M. Hughes, Eds., *Reviews in Mineralogy and Geochemistry* , 48, 13-49.
- Peroos, S., Du, Z., de Leeuw, N. H. (2006) A computer modeling study of the uptake, structure and distribution of carbonate defects in hydroxyl-apatite. *Biomaterials*, 27, 2150-2161.
- Roux, P., Bonel, G. (1980) Structural evolution of high pressure carbonated apatites. *Annales des Chimie France*, 6, 387 – 406.
- Tacker, R. C. (2008) Carbonate in igneous and metamorphic fluorapatite: Two type A and two type B substitutions. *American Mineralogist*, 93, 168-176.
- Vignoles, M., Bonel, G., Holcomb, D.W., Young, R.A., (1988) The influence of preparation conditions on the composition of type B carbonated hydroxyapatite and on the localization of the carbonate ions. *Calcified tissue international*, 43. 33-40.

Wallaeys, R. (1954) Study of carbonate apatite obtained by synthesis in the solid state. Silicon, sulphur, phosphates. Colloquium of the International Union of Pure and Applied Chemistry, Munster, Verlag Chemie, Weinheim, Germany, 183-190.

Weidner, V.L.; Carney, M.C.; Schermerhorn, D.V.; Pasteris, J.D.; Yoder, C.H. (2015) A-type substitution in carbonated strontium fluor-, chlor- and hydroxylapatites, Mineralogical Magazine, 79. 399-412.

Yoder, C.H., Bollmeyer, M.M., Stepien, K.R., Dudrick, R.N. (2019) The effect of incorporated carbonate and Na on the IR spectra of A-, B- and AB-type carbonated apatites, American Mineralogist, in review 2018.

Figure Captions

Figure 1. The IR spectra of the: (a) asymmetric stretch (ν_3) and (b) out-of-plane bend (ν_2) carbonate regions for low Na ^{13}C -CSrApOH (12).

Figure 2. The ^{13}C NMR solid-state MAS spectrum of low Na ^{13}C -CSrApOH (12).

Figure 3. The IR spectra of the (a) asymmetric stretch (ν_3), and (b) out-of-plane bend (ν_2) carbonate regions for high Na ^{13}C -CSrApOH (15).

Figure 4. The ^{13}C NMR solid-state MAS spectrum of high Na ^{13}C -CSrApOH (15).

Figure 5. The IR spectrum of the (a) asymmetric stretch (ν_3), and (b)) out-of-plane bend (ν_2) carbonate regions of ^{13}C -CSrApF (71).

Figure 6. The ^{13}C solid-state MAS NMR spectrum of ^{13}C -CSrApF (71).

Figure 7. The ^{13}C NMR solid-state MAS spectrum of ^{13}C -CSrApCl (57).

Figure 8. The ^{13}C NMR solid-state MAS spectrum of high Na ^{13}C -CSrApCl (58).

Figure 9. The A-site environment for carbonate in unit cell, after Fleet and Liu (2007) with planes containing three Sr^{2+} cations in each symmetry plane ($z = \frac{1}{4}$ and $\frac{3}{4}$).

Figure 10. Comparison of carbonate (ν_3) regions of the IR spectra of low Na CSrApOH (12), low NH_4^+ CSrApOH (64), low K CSrApOH (72), and high Na CSrApOH(15).

Figure 11. Top: The IR spectra of ν_3 region of carbonate in low Na CSrApOH (44) before (left) and after (right) heating to 600 °C for 12 h. Bottom: The ^{13}C NMR region of high Na CSrApF (75) before (left) and after (right) heating to 600 °C for 12 h.

Figure 12. Six-peak fit of the IR carbonate regions of calcium apatite (82) using the same model used for CSrApOH. (a) ν_3 region: (b) ν_2 region (Yoder, et al. in review 2018).

Tables

Table 1. IR band positions for the carbonate asymmetric stretch (ν_3) and out-of-plane bend (ν_2) regions and NMR ^{13}C chemical shifts of A-type carbonated Sr hydroxyl-, fluor- and chlorapatites (A-CSrApOH, A-CSrApF, A-CSrApCl).

Apatite	IR (ν_3), cm^{-1}	IR (ν_2) cm^{-1}	NMR, ppm
A-CSrApOH	1545, 1454	877	164.1
A- ^{13}C SrApOH	1508, 1415	851	164.1
A-CSrApF	1555, 1464	878	*
A-CSrApCl	1559, 1451	879	*

* NMR chemical shifts were not obtained on unlabeled apatites due to excessive total acquisition times.

Table 2. Band frequencies and populations for the carbonate asymmetric stretch (ν_3) and out-of-plane bend (ν_2) regions of the IR spectrum and the NMR.

Peak	ν_3 position, cm^{-1}	Population, %	ν_2 position, cm^{-1}	Population, %	Position, ppm	Population, %
Low Na ^{13}C-CSrApOH (12)						
A	1507, 1416	13	851*	15	165.2	17
A'	1474, 1381	14	854*	16	166.5	20
A''	1439, 1345	24	834	22	169.4	21
B	1396, 1365	49	844	47	167.9	42
High Na ^{13}C-CSrApOH (15)						
A	1508, 1415	5	850	5	166.2	5

A'	1469, 1381	15	853	20	167.5	19
A''	1428, 1351	44	843	39	169.5	44
B	1396, 1368	36	845	36	168.5	30
¹³C-CSrApF (71)						
A'	1435, 1382	22	847	26	168.9	33
A''	1412, 1363**	45	842	41	169.8	40
B	1397, 1380***	33	837	33	170.3	27
¹³C-CSrApCl (57)						
A	1512, 1414	15			165.1	19
A'	1477, 1396	10			165.6	14
A''	1441, 1382	35			169.3	26
B	1399, 1361	39			167.5	41
High Na ¹³C-CSrApCl (58)						
A	1509, 1417	4	850	6	165.8	4
A'	1469, 1390	17	853	18	167.0	18
A''	1431, 1355	47	843	46	169.5	31
B	1397, 1370	32	845	30	168.3	48

Numbers in parentheses are sample identifiers (ID).

*assignment arbitrary; **alternate 1412, 1380; ***alternate 1397, 1363

Table 3. Possible composition of the apatite channel after charge balance (Na as counter ion = sub) for B-type substitution.

	No subs	1 sub	2 sub	1 vacancy
--	---------	-------	-------	-----------

Channel		5 Sr	4 Sr	5 Sr
composition	6 Sr	1 Na	2 Na	1 vacancy
Charge/ unit				
cell	12	11	10	10
% Na *	0	1.7	3.6	0

*For B-type substitution of one mole CO₃ per mole Na.

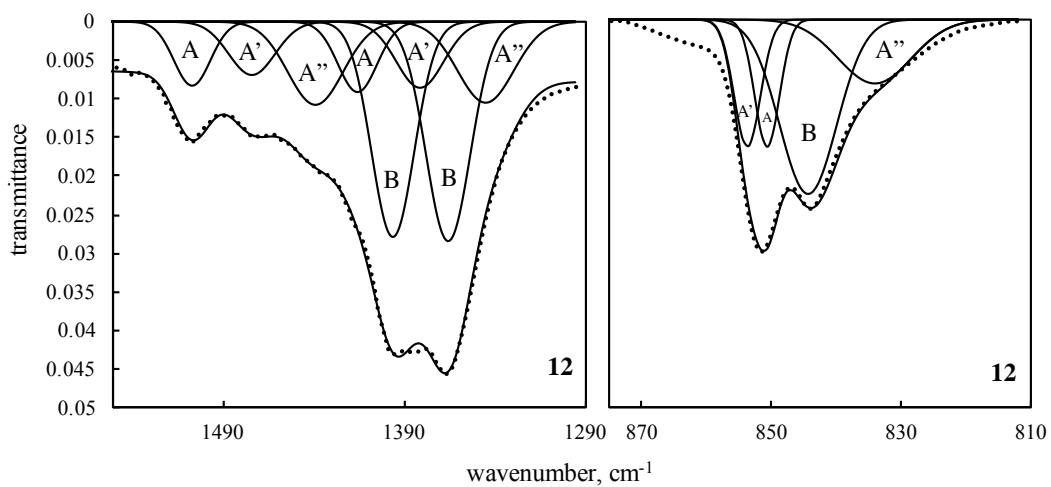
Table 4. Comparison of the populations of A- and B-type carbonate environments in low and high Na hydroxyl-, chlor- and fluorapatites. All apatites prepared using a 0.7 to 1 mole ratio of ¹³C- NaHCO₃ to phosphate.

	CSrApOH		CSrApCl		CSrApF	
	Low Na	High Na	Low Na	High Na	Low Na	High Na
	(12)	(15)	(57)	(58)	(65)	(71)
% CO ₃	4.4	7	3.7	7.4	2.2	3.2
% Na	0.8	1	0.4	0.8	0.3	0.6
A	15	5	15	6	0	0
A'	16	15	10	18	24	22
A''	22	44	35	46	37	45
B	47	37	39	30	39	33

Numbers in parentheses are sample identifiers (ID).

Figures

Figure 1



(a)

(b)

Figure 2

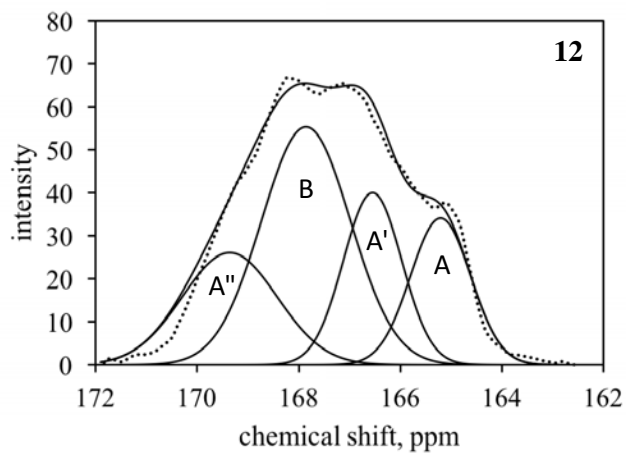


Figure 3

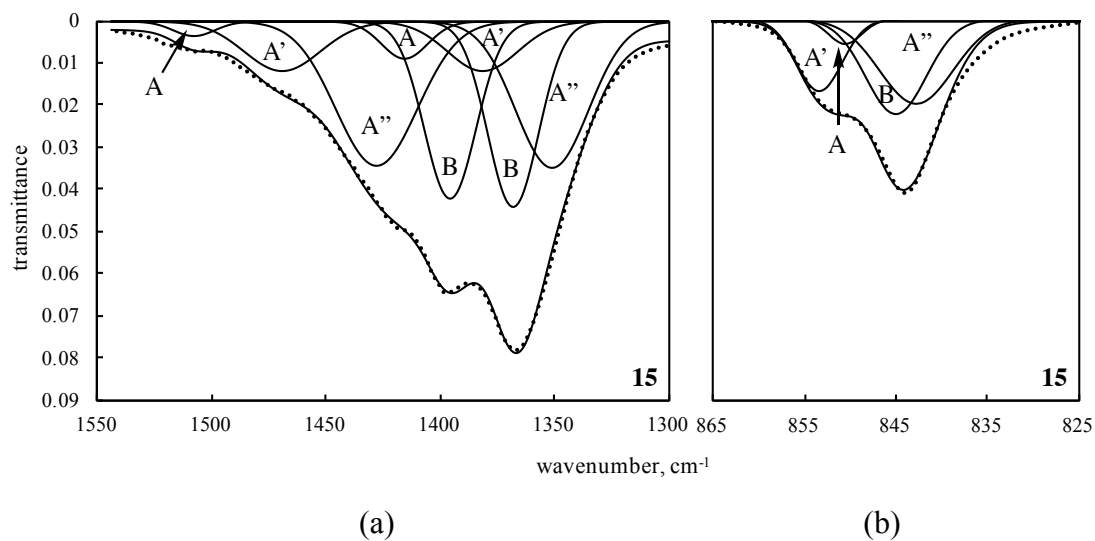


Figure 4

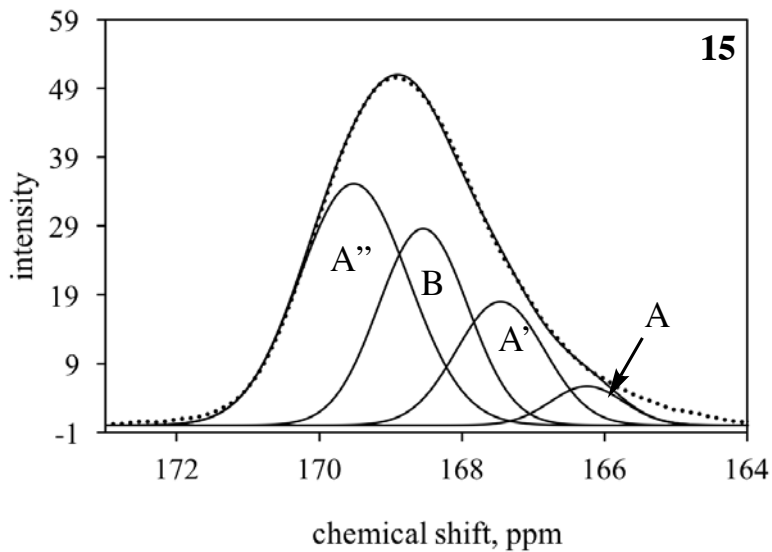
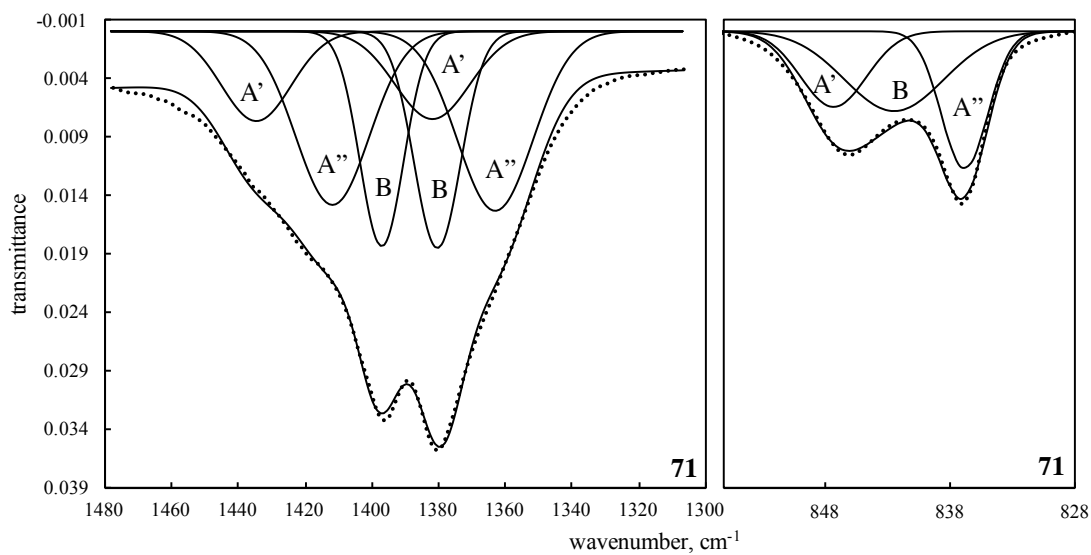


Figure 5



(a)

(b)

Figure 6

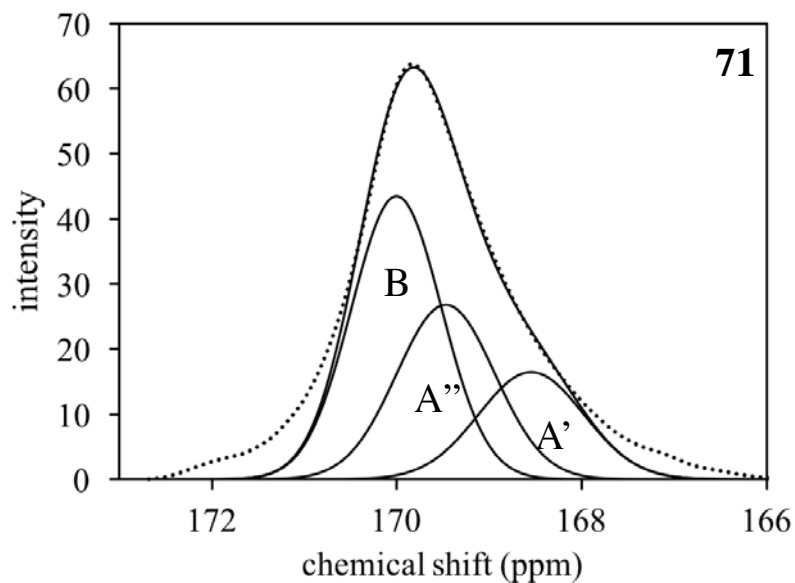


Figure 7

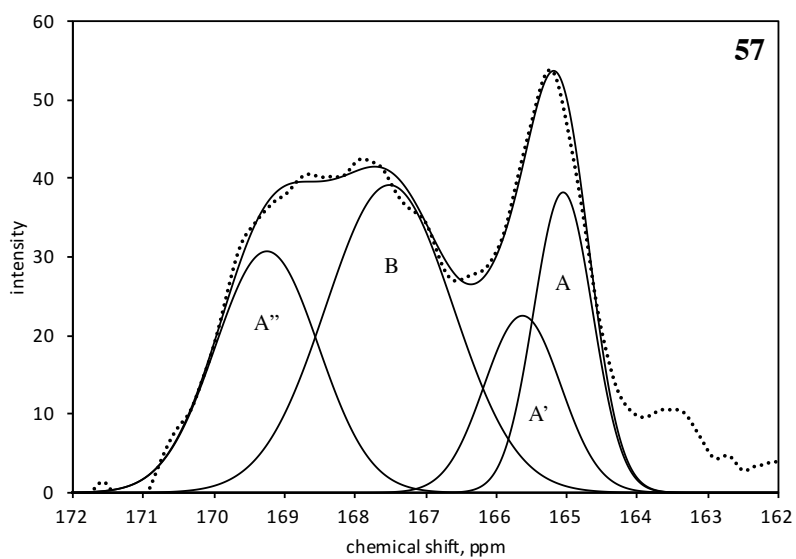


Figure 8

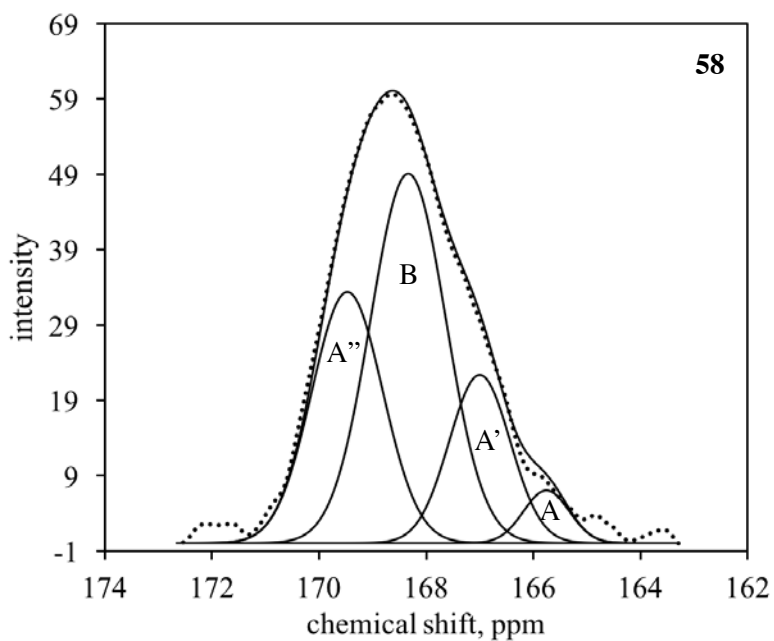


Figure 9

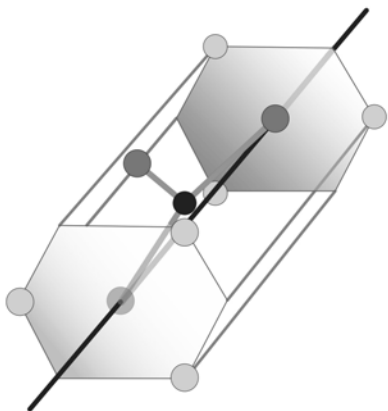


Figure 10

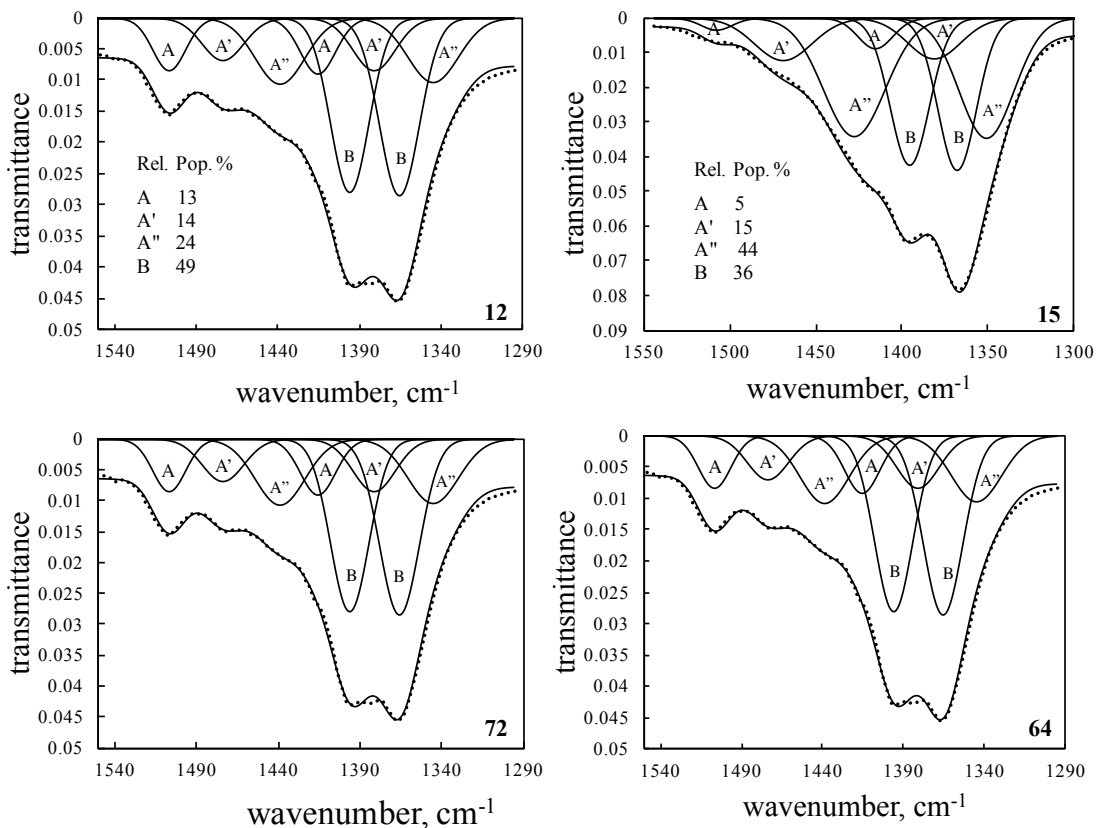


Figure 11

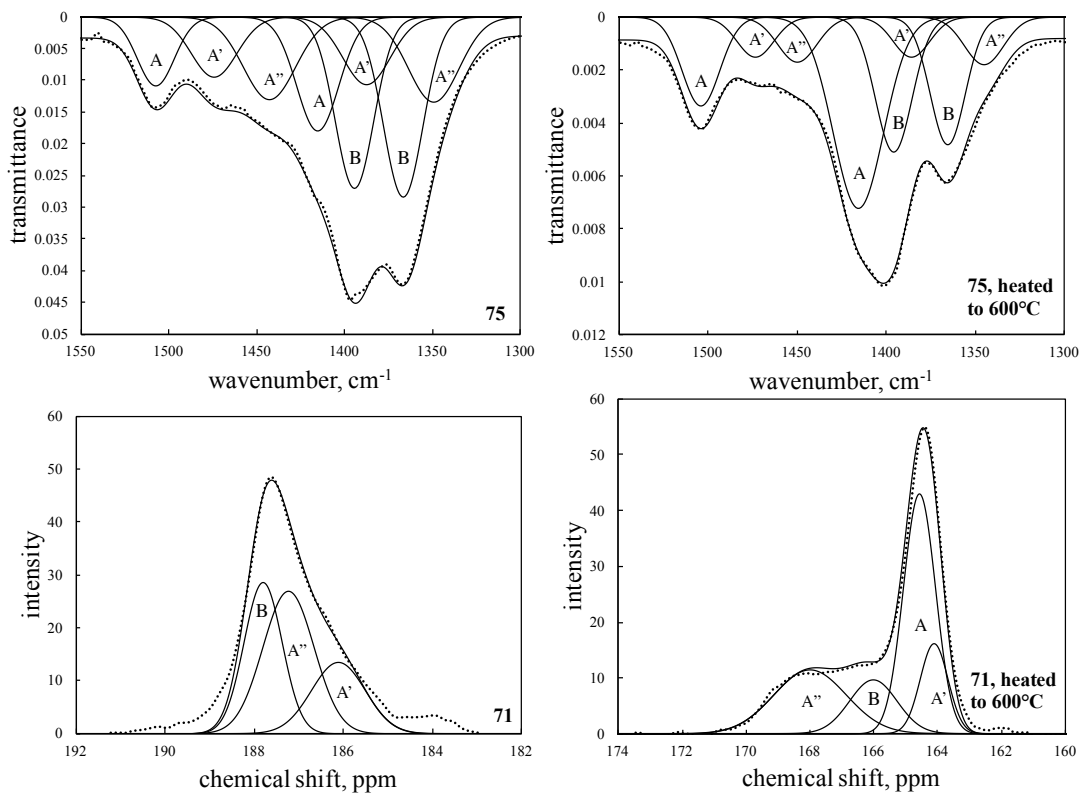


Figure 12

